Total Fractional-order Variation Regularization based Image Reconstruction Method for Capacitively Coupled Electrical Resistance Tomography

Yanyan Shi[a,b], Juanjuan Liao[a], Meng Wang[a,*], Mengge Li[a], Feng Fu[b,*], Manuchehr Soleimani[c]

[a] Department of Electronic and Electrical Engineering, Henan Normal University, Xinxiang, China, 453007

[b] College of Biomedical Engineering, Fourth Military Medical University, Xi'an, China, 710032

[c] Department of Electronic and Electrical Engineering, University of Bath, Bath, UK, BA2 7AY

*Corresponding author: Meng Wang, Feng Fu

Abstract: Compared with electrical resistance tomography, capacitively coupled electrical resistance tomography (CCERT) is preferred since it avoids problems of electrode corrosion and electrode polarization. However, reconstruction of conductivity distribution is still a great challenge in CCERT. To improve reconstruction quality, this work proposes a novel image reconstruction method based on total fractional-order variation regularization. Simulation work is conducted and reconstruction of several typical models is studied. Robustness of the proposed method to noise is also conducted. Additionally, the performance of the proposed reconstruction method is quantitatively evaluated. We have also carried out phantom experiment to further verify the effectiveness of the proposed method. The results demonstrate that the quality of reconstruction has been largely improved when compared with the images reconstructed by Landweber, Newton-Raphson and Tikhonov methods. The inclusion is more accurately reconstructed and the background is much clearer even under the impact of noise.

Keywords: capacitively coupled electrical resistance tomography, image reconstruction, total fractional-order variation regularization.

I. Introduction

Electrical resistance tomography (ERT) is an emerging imaging technique which has received considerable attention in monitoring multiphase flow [1-3]. Compared with other tomographic methods, ERT has the advantages of fast response, low cost, non-radiation and non-invasiveness [4],[5]. It is favorable for its visualization of conductivity distribution. However, sensor electrodes in ERT equipment are in contact with the measured medium. As a result, electrode corrosion and polarization is generated which affects measurement accuracy. Inspired by capacitively coupled contactless conductivity detection (C^4D), capacitively coupled electrical resistance tomography (CCERT) has been developed [6],[7]. It is a non-contact conductivity measurement method with which imaging of conductivity distribution can be also realized. In CCERT, an array of electrodes is installed outside the pipe at equal intervals. Since the electrodes are not contact with the medium in the pipe, the problems

of electrode corrosion and polarization in ERT can be avoided. It largely improves the system reliability and reduces the maintenance cost.

It should be remarked that image reconstruction is essential for conductivity reconstruction with CCERT. By processing the measured data from the electrodes, conductivity distribution in the detected region can be visualized with an image reconstruction method. It is known that reconstruction in ERT is mathematically a nonlinear ill-posed inverse problem. To cope with this problem, various methods have been proposed [8]-[11]. Similar with ERT, it is also a great challenge for the imaging of conductivity distribution with CCERT. Up until now, a number of methods have been proposed for image reconstruction in CCERT. In [12], a hybrid image reconstruction method with the combination of Tikhonov regularization and synchronous iterative reconstruction technique is presented for recovering conductivity distribution. In [13], image reconstruction in CCERT is implemented by combining Levenberg-Marquardt (L-M) method with synchronous algebraic reconstruction technique. With grey-level distribution of the image obtained by L-M method as the initial iterative value, the reconstruction is realized by employing synchronous algebraic reconstruction technique. In [14], an image reconstruction method combing linear back projection algorithm with K-means clustering algorithm is proposed. The linear back projection algorithm is used to obtain the original reconstructed image and the K-means clustering algorithm is used to obtain gray threshold values. Although some satisfactory results have been acquired, the reconstruction quality is still needed to be improved.

To solve a typical ill-posed inverse problem in electrical tomography, Tikhonov regularization is a classical approach [15]. By adding a smoothing regularization term, the ill-posed problem can be regularized and is converted into a well-posed problem. However, the edge of an image is not well preserved with this method [16]. Comparatively, total variation regularization tends to search solution of piecewise constant function and is advantageous for edge preservation [17]-[20]. The disadvantage is that blocky effect is yielded when reconstructing images with smooth edge [21]. Mathematically, the problem of total variation method can be addressed by introducing higher-order or fractional-order derivatives. The success of these methods has been demonstrated in the field of image processing [22]-[24]. In this work, a novel image reconstruction method based on total fractional-order variation regularization（TFVR） is proposed for recovering conductivity distribution in CCERT.

The remainder of this work is organized as follows. In section II, the mathematical model of CCERT is presented. The proposed TFVR method is provided in section III. In section IV, numerical simulation and phantom experiment are conducted to demonstrate the effectiveness of the proposed method. Also, comparison work with other reconstruction methods is performed. Section V draws the conclusion.

II. Mathematical model of CCERT

A typical CCERT measurement system is mainly composed of an array of sensor electrodes, a data acquisition and processing unit, and an image reconstruction unit. Fig. 1 shows the arrangement of electrodes in CCERT and its equivalent excitation-measurement circuit. As shown in Fig. 1(a), twelve electrodes are equidistantly equipped around an insulating pipe filled with conductive medium. With one electrode excited by an alternating voltage and one electrode performed as a measurement terminal, an AC path is established between the two electrodes [25]. The equivalent circuit is illustrated in Fig. 1(b). C_{p1} and C_{p2} denote the coupling capacitance between two electrodes while R_m represents the equivalent resistance of conductive medium. Note that the current measured from the detection electrode reflects medium conductivity. Based on the measurement obtained by the data acquisition and processing unit, conductivity distribution is visualized with the image reconstruction unit.

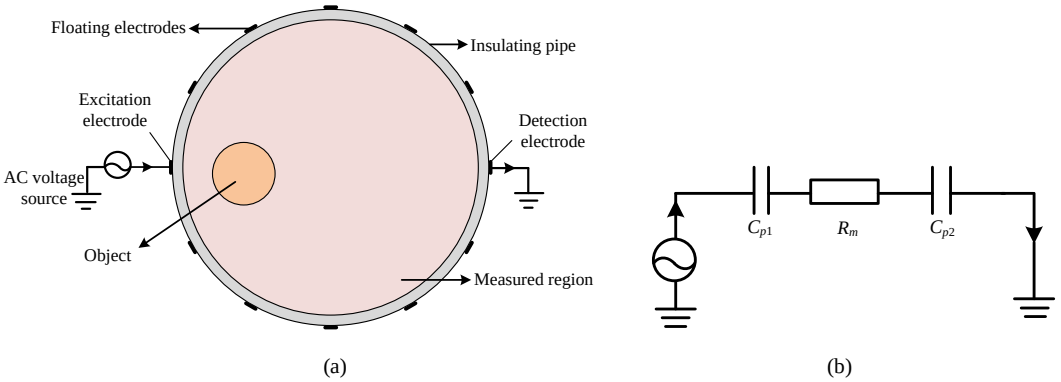

Fig.1 (a)The sketch of a 12-electrode CCERT sensor (b)Equivalent circuit of an electrode pair.

The electrode is excited at the frequency of 500 kHz. Since the wavelength of the excitation signal is much larger than the dimension of the detected region, the sensitive field in CCERT is a quasi-static electromagnetic field. Based on Maxwell equations, the relationship between potential distribution and electrical parameters is mathematically described by [26]:

$$\nabla\left(\left(\sigma(x,y)+jw\varepsilon(x,y)\right)\nabla\psi(x,y)\right)=0 \quad (x,y)\subseteq\Omega \tag{1}$$

where $\sigma(x,y)$ represents conductivity distribution, $\varepsilon(x,y)$ and $\psi(x,y)$ are respectively spatial permittivity and potential distribution, and Ω denotes the sensing area.

Boundary conditions are expressed by

$$\begin{aligned} &\psi_i(x,y)=V_0 \quad (x,y)\subseteq\Gamma_i \\ &\psi_j(x,y)=0 \quad (x,y)\subseteq\Gamma_j \\ &\frac{\partial\psi_k(x,y)}{\partial n}=0 \quad (x,y)\subseteq\Gamma_k\,(k\neq i,j) \end{aligned} \tag{2}$$

where i, j and k are the indexes of excitation electrode, detection electrode and floating electrodes, respectively; V_0 is the sinusoidal excitation voltage; Γ_i , Γ_j , Γ_k represent the spatial locations of excitation electrode, detection electrode and floating electrodes, respectively; n denotes outward unit normal vector.

The current I_{ij} measured on the detection electrode can be obtained by[27]

$$I_{ij}=\int_{\Gamma} J\cdot d\Gamma \tag{3}$$

where J represents current density near the electrode.

The equivalent impedance Z_{ij} between the excitation and detection electrode pairs can be calculated. It is worth noting that only the real part of Z_{ij} represents the equivalent resistance between electrodes which reflects the conductivity. Therefore

$$\begin{aligned} Z_{ij}&=\frac{V_0}{I_{ij}} \\ R_{ij}&=\mathrm{Re}\left(Z_{ij}\right) \end{aligned} \tag{4}$$

where R_{ij} is the equivalent resistance between electrode pairs i and j.

Based on finite element method, the variation of equivalent resistance ΔR against conductivity change $\Delta\sigma$ can be described by

$$\Delta R=S\Delta\sigma \tag{5}$$

where S represents sensitivity matrix, which reflects the change of resistance caused by conductivity variation in the measured domain [28].

For simplicity, (5) is rewritten as

$$H=Sg \tag{6}$$

where H represents ΔR and g stands for $\Delta\sigma$.

III. Image Reconstruction based on Total Fractional-order Variation Regularization

It can be found from (6) that conductivity distribution in the detected region can be calculated once resistance and sensitivity matrix are known. In this paper, a novel total fractional-order variation

regularization (TFVR) strategy is proposed for image reconstruction in CCERT. To cope with the ill-posedness of reconstruction, a fractional-order regularization term is added to restrict the solution. During the reconstruction, the proposed TFVR strategy is mathematically modeled as

$$\hat{g}=\arg\min_{g}\left\{\frac{\lambda}{2}\left\|Sg-H\right\|_2^2+\left\|D^p g\right\|_1\right\} \tag{7}$$

where $\hat{g}$ is the estimated optimal conductivity, D^p is the pth order finite difference, and λ is the regularization parameter used to balance the fidelity term and the regularization term.

Eq. (7) can be expressed as

$$\hat{g}=\arg\min_{g}\left\{\frac{\lambda}{2}\left\|Sg-H\right\|_2^2+\left\|w\right\|_1\right\}\quad D^p g=w \tag{8}$$

Due to non-differentiability and nonlinearity of (8), it is still difficult to solve directly and effectively. Therefore, iterative alternating minimization scheme in [29] is introduced to obtain the solution of inverse problem. The minimized augmented Lagrangian function of (8) is

$$\min_{w,g} L_A\left(w,g\right)=\left\|w\right\|-v^T\left(D^P g-w\right)+\frac{\beta}{2}\left\|D^P g-w\right\|_2^2-\lambda^T\left(Sg-H\right)+\frac{\mu}{2}\left\|Sg-H\right\|_2^2 \tag{9}$$

Based on alternating direction method in [30],[31], (9) is decomposed into two simple sub-problems:

$$\begin{cases}\min\limits_{w}\left\|w\right\|-v^T\left(D^p g_m-w\right)+\dfrac{\beta}{2}\left\|D^p g_m-w\right\|_2^2\\ \min\limits_{g}\xi_m\left(g\right)\triangleq -v^T\left(D^p g-w_{m+1}\right)+\dfrac{\beta}{2}\left\|D^p g-w_{m+1}\right\|_2^2-\lambda^T\left(Sg-H\right)+\dfrac{\mu}{2}\left\|Sg-H\right\|_2^2\end{cases} \tag{10}$$

For the w sub-problem, the solution is given by

$$w_{m+1}=\max\left(\left\|D^p g_m-\frac{v}{b}\right\|-\frac{1}{b},0\right)\frac{D^p g_m-\dfrac{v}{b}}{\left\|D^p g_m-\dfrac{v}{b}\right\|} \tag{11}$$

The g sub-problem is solved by:

$$g_{m+1}=\left(\beta\left(D^p\right)^T D^p+\mu S^T S\right)^{+}\left(\left(D^p\right)^T v+\beta\left(D^p\right)^T w_{m+1}+S^T\lambda+\mu S^T H\right) \tag{12}$$

Besides, the one-step steepest descent method is adopted to obtain the final solution as:

$$g_{m+1}=g_m-\alpha_m d_m \tag{13}$$

in which the step length is calculated by

$$\alpha_m=\frac{Z_m^T Z_m}{Z_m^T y_m}$$

where d is the gradient direction of the objective function.

Note that

$$Z_m=g_m-g_{m-1} \tag{14}$$

$$y_m=d_m\left(g_m\right)-d_m\left(g_{m+1}\right)$$

During the iteration, the nonmonotone Armijo condition is required which is expressed as

$$\xi_m\left(g_m-\alpha_m d_m\right)\le C_m-\delta\alpha_m d_m^T d_m \tag{15}$$

in which

$$C_{m+1}=\frac{\eta P_m C_m+\xi_m\left(g_{m+1}\right)}{P_{m+1}}$$
$$P_{m+1}=\eta P_m+1$$

where η and δ are selected between 0 and 1.

To summarize, the proposed TFVR strategy for image reconstruction in CCERT can be solved by alternating minimization scheme which is tabulated in Algorithm 1.

Algorithm 1: The solution for the proposed TFVR strategy

Input: S, H, m, δ , ρ , η , w_0, g_0.

Initialize: $0<\delta,\rho,\eta<1$, $C_0=L_A\left(w_0,g_0\right)$.

Iterations:

1. **While** inner stopping condition unsatisfied **do**
2. Compute w_{m+1} using (11);
3. Set α_m through formula (13);
4. **While** formula (15) unsatisfied **do**
5. Backtrack $\alpha_m=\rho\alpha_m$;
6. **End do**
7. Compute g_{m+1} by one-step steepest descent method (13);
8. Set C_{m+1} according (15);
9. m=m+1
10. **End do**

Output: g_{m+1}

IV. Simulation and Experimental Reconstruction

A. Simulation work

With the proposed TFVR strategy, image reconstruction in CCERT is conducted by simulation work. In the simulation, a circular region with inner diameter of 50 mm and outer diameter of 54 mm is constructed in Comsol MultiPhysics. Twelve electrodes are equidistantly installed outside the circular

region and inclusions are located in the detected area. The conductivity of the background and the inclusions is set to 0.03 S/m and 0.001 S/m, respectively. With an alternating voltage injected to an electrode, the equivalent resistance is calculated from another electrode while other electrodes are set to floating potential. There are totally 132 measurement data. The sensitivity matrix is preliminarily obtained. Based on the calculated sensitivity matrix and the measured resistance, conductivity distribution is reconstructed with the proposed TFVR method implemented in Matlab R2016a. In addition, image reconstructions obtained by Landweber, Newton-Raphson and Tikhonov methods are performed and used for comparison.

In the study, six different models are reconstructed. The inclusion in the models has the same conductivity. These models cover inclusions with different quantities, different sizes and different locations. The image reconstructed by the TFVR method is shown in Fig. 3. Also, the reconstruction is compared with the results of Landweber, Newton-Raphson and Tikhonov methods.

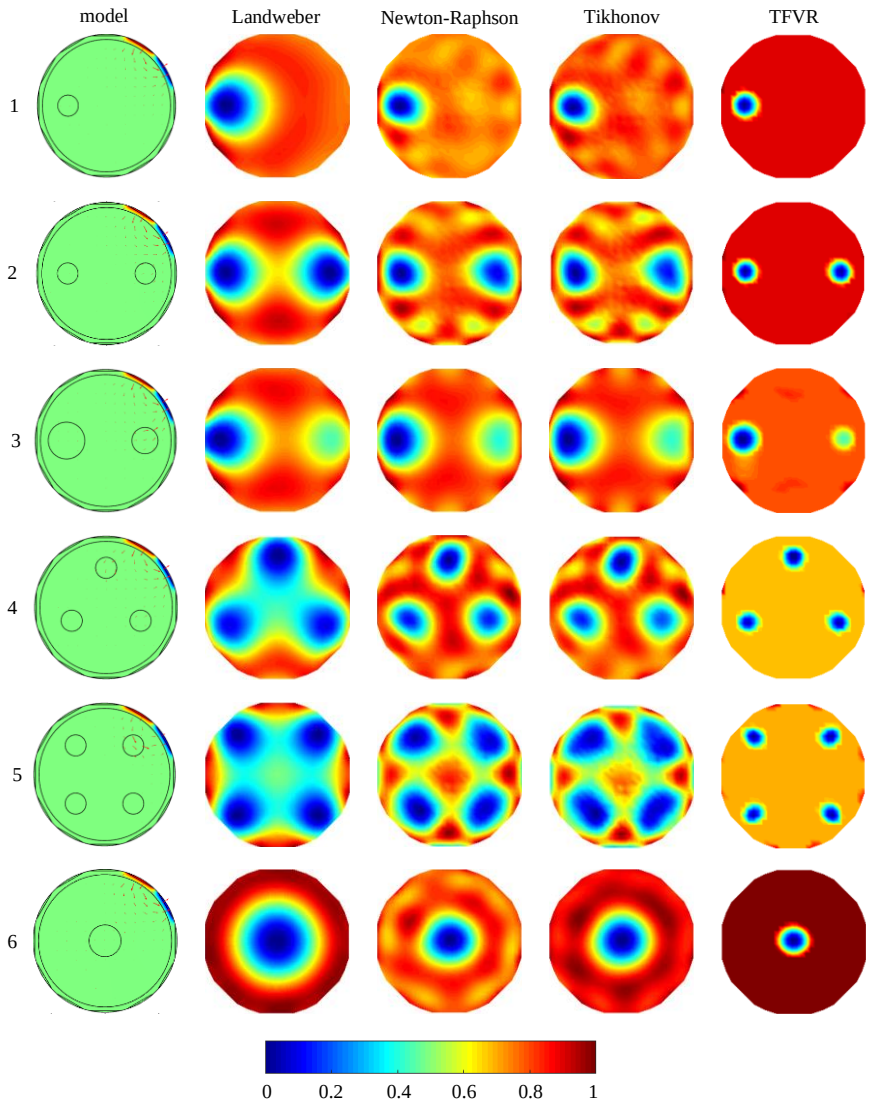

Fig. 3 Image reconstruction of different models without noise

From Fig. 3, it can be observed that the quality of images reconstructed by Landweber method is the worst. The reconstructed inclusion tends to be much larger than the original object. For models when there are multiple inclusions in the detected region, the boundary of inclusions can not be clearly identified from the reconstructed image. Moreover, the solution is not very accurate because this method is semi-convergent and the optimal solution may not be found. Compared with Landweber method, images reconstructed by Newton-Raphson method are generally improved. The boundary is clearer and it is easier to identify the boundary between inclusions. Images recovered by Tikhonov method are similar with the results of Newton-Raphson method. However, it takes much less time for the reconstruction with Tikhonov method. Note that the inclusions are still not well reconstructed and there are obvious artifacts in the reconstructed images. Comparatively, images reconstructed by the proposed TFVR method have been largely improved. The inclusion is the most accurately

reconstructed among the four methods. Moreover, the boundary of the inclusion is the clearest and almost no artifact is observed in the background.

For quantitative estimation of the proposed method in the reconstruction, blur radius (BR) is introduced to evaluate artifacts. It is defined as

$$BR = \sqrt{\frac{A_0}{A}} \tag{16}$$

where A_0 is the area of the reconstructed inclusion and A is the whole detected area[32].

TABLE 1 compares the calculated BR values when the reconstruction is conducted with the four methods. From (16), it can be found that a smaller BR value indicates fewer artifacts and higher reconstruction quality. Among the four methods, the proposed method shows the lowest BR values for all the six models. It further proves the excellent performance of this method in image reconstruction.

TABLE1 Comparison of blur radius values with different methods

model \ Method	Landweber	Newton-Raphson	Tikhonov	TFVR
1	0.4312	0.3747	0.3562	0.1823
2	0.5830	0.5264	0.5000	0.2301
3	0.5061	0.4629	0.4508	0.2506
4	0.7681	0.6248	0.6058	0.2579
5	0.8773	0.6714	0.6452	0.2741
6	0.5702	0.4938	0.4799	0.2046

It is also of great importance to estimate computing time of the image reconstruction method. In TABLE 2, time performance of Landweber, Newton-Raphson and Tikhonov methods and the proposed method are compared. Since Tikhonov method requires no iteration, the reconstruction costs the shortest time. Newton-Raphson method takes the longest time as multiple iterations are required. Comparatively, calculation time of the proposed method is a little longer than that of Tikhonov method.

TABLE2 Comparison of time performance with different methods

model \ Method	Landweber	Newton-Raphson	Tikhonov	TFVR
1	0.1467	0.4681	0.0128	0.0828
2	0.1392	0.4560	0.0126	0.0809
3	0.1358	0.4630	0.0138	0.0817
4	0.1345	0.4592	0.0142	0.0810
5	0.1355	0.4655	0.0129	0.0825
6	0.1383	0.4551	0.0132	0.0803

It is known that it is difficult to reconstruct inclusions with different conductivity. Aside from reconstruction of inclusions with the same conductivity, it is also essential to study the performance of the proposed method in reconstructing inclusions with different conductivity. Fig. 4 shows reconstruction of a model with the four methods. In this model, two inclusions respectively having the conductivity of 0.001 S/m and 0.005 S/m are positioned in the detected region. As can be seen from Fig. 4, the image reconstructed by the proposed method is obviously much better than other three regularization methods. The inclusion is the most accurately reconstructed. Also, the background is the clearest and no artifacts are observed.

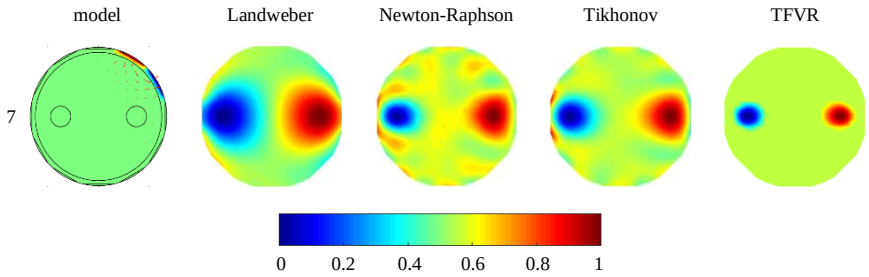

Fig.4 Reconstruction of a model with inclusions having different conductivity

It should be noted that noise has a great impact on the measurement. To evaluate the anti-noise performance of the proposed TFVR method in the image reconstruction, Gaussian white noise with a noise level of 1% is considered to simulate an actual CCERT system. Under the noise, the reconstruction result is shown in Fig. 5. It is obvious that the images reconstructed by the four methods are affected by the noise. In some reconstructions, the recovered inclusions are deformed and more artifacts are observed. Nevertheless, the TFVR method proposed in this work shows the strongest robustness to the noise among the four methods. The inclusion is still the best reconstructed and the background shows the fewest artifacts.

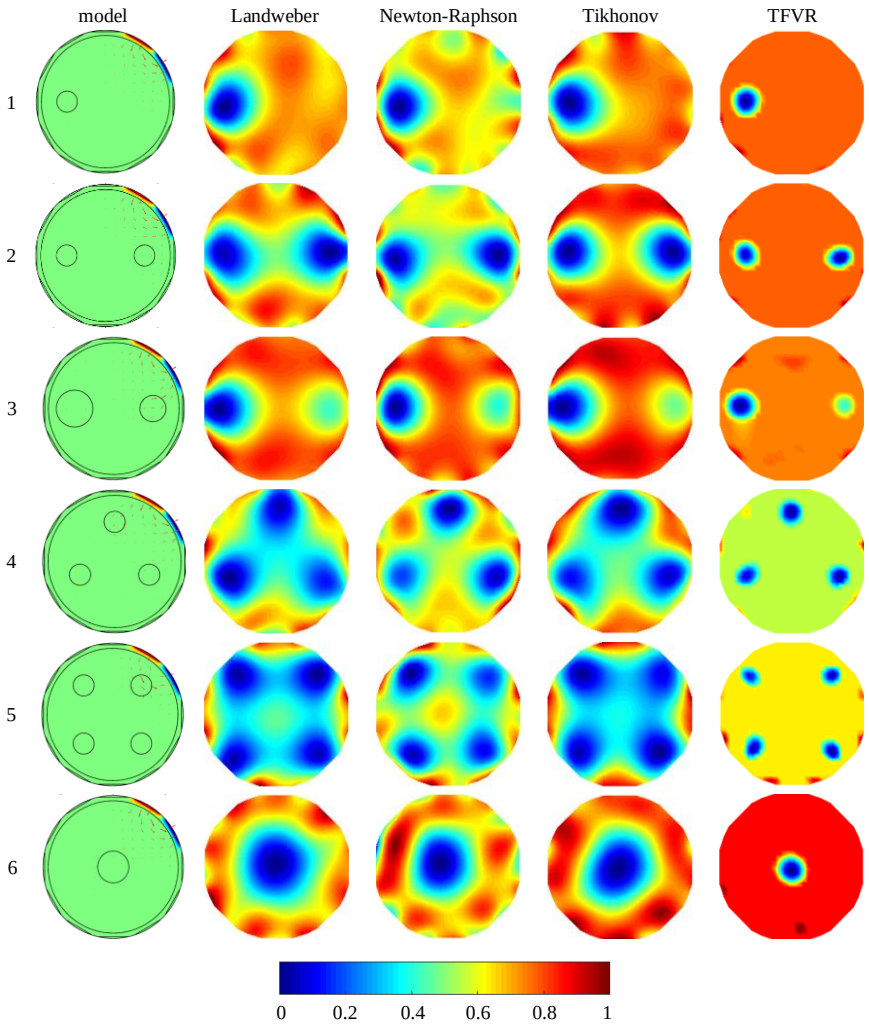

Fig.5 Image reconstruction under noise level of 1%

Under the noise level of 1%, TABLE 3 compares the BR values when reconstruction of six models is performed with the four methods. Again, the proposed TFVR method shows the smallest BR value among these methods which further demonstrates the robustness of this method to noise.

TABLE 3 Comparison of blur radius values under noise level of 1%

Method / model	Landweber	Newton-Raphson	Tikhonov	TFVR
1	0.4773	0.4589	0.4298	0.1683
2	0.6099	0.5659	0.5648	0.2135
3	0.5205	0.5000	0.4988	0.2163
4	0.7728	0.6058	0.7453	0.2531
5	0.8710	0.7616	0.8200	0.2718
6	0.6877	0.6078	0.6209	0.1985

In addition, Fig. 6 shows the anti-noise performance of the proposed TFVR method in reconstructing inclusion with different conductivity. Reconstructed images are compared with the results obtained by

Landweber, Newton-Raphson and Tikhonov methods. It is found that the shape of inclusions can be much better reconstructed by the TFVR method and the reconstruction is less affected by noise. Comparatively, serious deformation of inclusions is generated and lots of artifacts are observed in the reconstructed images of other three methods.

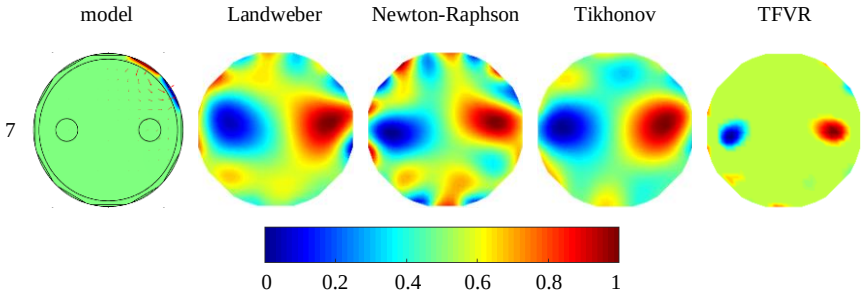

Fig.6 Image reconstruction of inclusions with different conductivity under noise level of 1%

B. Phantom experimental validation

To validate the feasibility and effectiveness of the proposed TFVR image reconstruction algorithm, we carried out phantom experiments on a 12-electrode CCERT system [33]. The tank is filled by tap water with the conductivity of 0.018 S/m. Several combinations of plastic rods with the diameter of 26.5 mm, 29.5 mm and 34.5 mm are employed as the inclusion. The frequency and amplitude of the excitation voltage are 500 kHz and 3.3V respectively. Fig. 7 shows the reconstruction results. Also, comparison is made with the images reconstructed by Landweber, Newton-Raphson and Tikhonov methods. From Fig. 7, it can be observed that the proposed TFVR method outperforms other three methods during the reconstruction of conductivity distribution. The reconstructed object is the most similar with the true inclusion. Furthermore, the boundary of inclusions is the clearest and the artifacts in the background are the least.

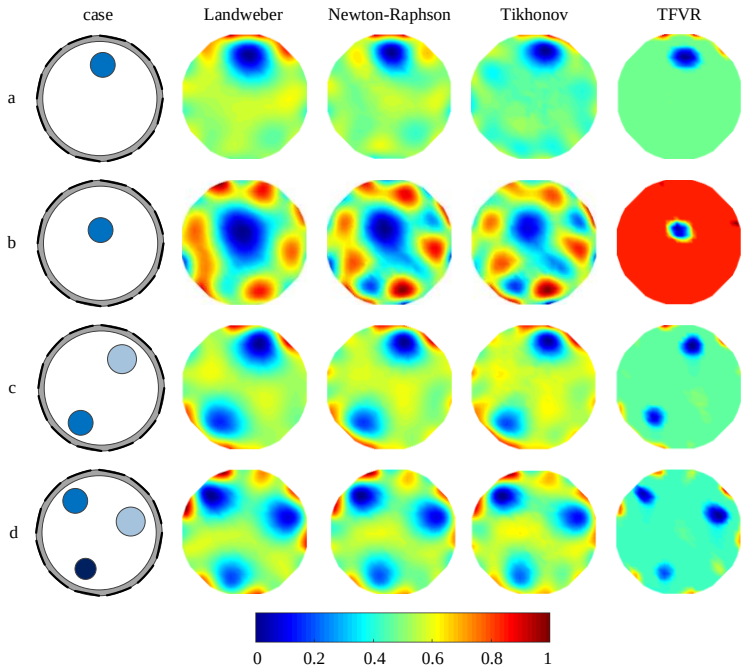

Fig.7 Reconstructed images based on experimental cases

V. Conclusion

In this paper, a novel TFVR method is proposed for recovering conductivity distribution in CCERT. According to the measurement principle, the mathematical model of CCERT is firstly established. To acquire conductivity distribution, iterative alternating minimization scheme is adopted to solve the proposed method. To verify the performance of the proposed TFVR strategy, reconstruction of several typical models with inclusions having the same conductivity is studied by simulation work. An additional model with inclusions having different conductivity is also studied. The results show that images reconstructed by the proposed method are obviously much better than other three regularization methods. By introducing the concept of blur radius, quantitative evaluation of the proposed method in inhibiting artifacts is conducted. It is found that BR values of the proposed method are the lowest which indicates the fewest artifacts and highest reconstruction quality. Calculation time of the proposed method is acceptable. Furthermore, anti-noise performance of the four methods is compared and the strongest robustness to noise is observed for the proposed TFVR method. Phantom experiments demonstrate the effectiveness of the proposed method.

Acknowledgement

This work is supported in part by National Natural Science Foundation of China under Grant 61903127 and 51837011, in part by Postdoctoral Research Foundation of China under Grant

2020M673664, and in part by Scientific and Technological Innovation Program for Universities in Henan Province of China under Grant 21HASTIT018.

REFERENCES

[1]. R. Kotze, A. Adler, A. Sutherland, C.N. Deba, Evaluation of electrical resistance tomography imaging algorithms to monitor settling slurry pipe flow, *FLOW MEASUREMENT AND INSTRUMENTATION*, 2019,68:101572.

[2]. H.R. Wang, J.B. Jia, Y.J. Yang et al., Quantification of gas distribution and void fraction in packed bubble column using electrical resistance tomography, *IEEE SENSORS JOURNAL*, 2018,18(21):8963-8970.

[3]. G. Annamalai, S. Pirouzpanah, S.R. Gudigopuram, G.L. Morrison, Characterization of flow homogeneity downstream of a slotted orifice plate in a two-phase flow using electrical resistance tomography, *FLOW MEASUREMENT AND INSTRUMENTATION*, 2016,50:209-215.

[4]. M.A. Sattar, M.M. Garcia, R. Banasiak et al., Electrical resistance tomography for control applications: quantitative study of the gas-liquid distribution inside a cyclone, *SENSORS*, 2020,20(21): 6069.

[5]. F. Maluta, G. Montante, A. Paglianti, Analysis of immiscible liquid-liquid mixing in stirred tanks by Electrical Resistance Tomography, *CHEMICAL ENGINEERING SCIENCE*, 2020,227:115898.

[6]. P.C. Hauser, P. Kuban, Capacitively coupled contactless conductivity detection for analytical techniques - developments from 2018 to 2020, *JOURNAL OF CHROMATOGRAPHY A*, 2020,1632:461616.

[7]. Y.X. Wang , B.L. Wang, Z.Y. Huang et al., New capacitively coupled electrical resistance tomography (CCERT) system, *MEASUREMENT SCIENCE AND TECHNOLOGY* , 2018,29(10):104007.

[8]. S.J. Ren, Y. Wang, G.H. Liang, F. Dong, A robust inclusion boundary reconstructor for electrical impedance tomography with geometric constraints, *IEEE TRANSACTIONS ON INSTRUMENTATION AND MEASUREMENT*, 2019,68(3): 762-773.

[9]. F. Li, C. Tan, F. Dong, Electrical resistance tomography image reconstruction with densely connected convolutional neural network, *IEEE TRANSACTIONS ON INSTRUMENTATION AND MEASUREMENT*, 2021,70:4500811.

[10]. S.J. Ren, K. Sun, D. Liu, F. Dong, A statistical shape constrained reconstruction framework for electrical impedance tomography, *IEEE TRANSACTIONS ON MEDICAL IMAGING*, 2019,38(10):2400-2410.

[11]. Y.Y. Shi, X. Zhang, Z.G. Rao, Reduction of staircase effect with total generalized variation regularization for electrical impedance tomography, *IEEE SENSORS JOURNAL*, 2019,19(21):9850-9858.

[12]. B.L. Wang, W.H. Tan, Z.Y. Huang et al., Image reconstruction algorithm for capacitively coupled electrical resistance tomography, *FLOW MEASUREMENT AND INSTRUMENTATION*, 2014,40: 216-222.

[13]. W.H. Tan, B.L. Wang, Z.Y. Huang et al., New image reconstruction algorithm for capacitively coupled electrical resistance tomography. *IEEE SENSORS JOURNAL*, 2017,17(24):8234-8241.

[14]. Y.X. Wang , H.F. Ji, Z.Y. Huang et al., Study on image reconstruction of capacitively coupled electrical impedance tomography (CCEIT), *MEASUREMENT SCIENCE AND TECHNOLOGY*, 2019,30(9): 094002.

[15]. Y.B. Xu, Y. Pei, F. Dong, An adaptive Tikhonov regularization parameter choice method for electrical resistance tomography, *FLOW MEASUREMENT AND INSTRUMENTATION*, 2016,50:1-12.

[16]. X.Z. Song, Y.B. Xu, F. Dong, A hybrid regularization method combining Tikhonov with total variation for electrical resistance tomography, *FLOW MEASUREMENT AND INSTRUMENTATION*, 2015,46:268-275.

[17]. Y.Y. Shi, Z.G. Rao, C. Wang et al., Total variation regularization based on iteratively reweighted least-squares method for electrical resistance tomography, *IEEE TRANSACTIONS ON INSTRUMENTATION AND MEASUREMENT*, 2020,69(6):3576-3586.

[18]. B. Chen, J.F.P.J. Abascal, M. Soleimani, Electrical resistance tomography for visualization of moving objects using a spatiotemporal total variation regularization algorithm, *SENSORS*, 2018,18(6):1704.

[19]. Y.J. Yang, H.C. Wu, J.B. Jia, Image reconstruction for electrical impedance tomography using enhanced adaptive group sparsity with total variation, *IEEE SENSORS JOURNAL*, 2017,17(17):5589-5598.

[20]. A. Javaherian, M. Soleimani, K. Moeller et al., An accelerated version of alternating direction method of multipliers for TV minimization in EIT, *APPLIED MATHEMATICAL MODELLING*, 2016,40(21-22):8985-9000.

[21]. Y.Y. Shi, X.L. Kong, M. Wang et al., A non-convex L_1-norm penalty-based total generalized variation model for reconstruction of conductivity distribution, *IEEE SENSORS JOURNAL*, 2020,20(14):8137-8146.

[22]. P.F. Liu, Hybrid higher-order total variation model for multiplicative noise removal, *IET IMAGE PROCESSING*, 2020,14(5):862-873.

[23]. J.H. Yang, X.L. Zhao, T.H. Ma et al., Remote sensing images destriping using unidirectional hybrid total variation and nonconvex low-rank regularization, *JOURNAL OF COMPUTATIONAL AND APPLIED MATHEMATICS*, 2020,363:124-144.

[24]. M. Henriques, D. Valerio, P. Gordo, R. Melicio, Fractional-order colour image processing, *MATHEMATICS*, 2021,9(5):457.

[25]. Y.X. Wang, X.K. He, Y.D. Jiang et al., New image reconstruction algorithm for CCERT: LBP plus Gaussian mixture model (GMM) clustering, *MEASUREMENT SCIENCE AND TECHNOLOGY*, 2021,32(2):024001.

[26]. Y.D. Jiang, X.K. He, B.L. Wang et al., On the performance of a capacitively coupled electrical impedance tomography sensor with different configurations, *SENSORS*, 2020,20(20):5787.

[27]. B.L. Wang, W.B. Zhang, Z.Y. Huang et al., Modeling and optimal design of sensor for capacitively coupled electrical resistance tomography system, *FLOW MEASUREMENT AND INSTRUMENTATION*, 2013,31:3-9.

[28]. Y.D. Jiang, M. Soleimani, B.L. Wang, Contactless electrical impedance and ultrasonic tomography: correlation, comparison and complementarily study, *MEASUREMENT SCIENCE AND TECHNOLOGY*, 2019,30(11):114001.

[29]. S. Bartels, M. Milicevic, Efficient iterative solution of finite element discretized nonsmooth minimization problems, *COMPUTERS & MATHEMATICS WITH APPLICATIONS*, 2020,80(5): 588-603.

[30]. J.C. Bai, Y.X. Ma, H. Sun, M. Zhang, Iteration complexity analysis of a partial LQP-based alternating direction method of multipliers, *APPLIED NUMERICAL MATHEMATICS*, 2021,165:500-518.

[31]. J.J. Zhang, J.G. Nagy, An effective alternating direction method of multipliers for color image restoration, *APPLIED NUMERICAL MATHEMATICS*, 2021,164:43-56.

[32]. A. Adler, J.H. Arnold, R. Bayford et al., GREIT: a unified approach to 2D linear EIT reconstruction of lung images, *PHYSIOLOGICAL MEASUREMENT*, 2009,30(6):S35-S55.

[33]. Z.R. Chen, G.G. Ma, Y.D. Jiang et al., Application of deep neural network to the reconstruction of two-phase material imaging by capacitively coupled electrical resistance tomography, *ELECTRONICS*, 2021,10:1058.